2000-GT-497

ANALYSIS OF THE INTER-ROW FLOW FIELD WITHIN A TRANSONIC AXIAL COMPRESSOR : PART 2 – UNSTEADY FLOW ANALYSIS

Xavier Ottavy, Isabelle Trébinjac, André Vouillarmet
Ecole Centrale de Lyon
Laboratoire de Mécanique des Fluides et d'Acoustique
UMR CNRS 5509 / ECL / UCB Lyon I
69131 Ecully Cedex, France

ABSTRACT

An analysis of the experimental data, obtained by laser two-focus anemometry in the IGV-rotor inter-row region of a transonic axial compressor, is presented with the aim of improving the understanding of the unsteady flow phenomena. A study of the IGV wakes and of the shock waves emanating from the leading edge of the rotor blades is proposed. Their interaction reveals the increase in magnitude of the wake passing through the moving shock. This result is highlighted by the streamwise evolution of the wake vorticity. Moreover, the results are analyzed in terms of a time averaging procedure and the purely time-dependent velocity fluctuations which occur are quantified. It may be concluded that they are of the same order of magnitude as the spatial terms for the inlet rotor flow field. That shows that the temporal fluctuations should be considered for the 3D rotor time-averaged simulations.

NOMENCLATURE

Symbols

M_R = relative Mach number
N = number of blades
P = measurement point location
T = temporal period
$\vec{U}, U$ = rotor velocity vector, modulus
$\vec{V}, V$ = velocity vector, modulus
X = some flow parameter or other
$\vec{f}$ = external forces
n = co-ordinate normal to the shock
p = pressure
r = radial co-ordinate
t = time
z = axial co-ordinate
$\vec{\Omega}, \Omega$ = vorticity vector, modulus

Θ = angular blade pitch

α = absolute velocity angle
φ = phase shift
ω = rotation speed (radian/s)
θ = azimuthal co-ordinate
ρ = fluid density
$\overline{\overline{\tau}}$ = turbulent and viscous stress tensor
τ = co-ordinate tangent to the shock

Superscripts

— = time averaged value
~ = spatial averaged value
' = time fluctuating value in the absolute frame
* = spatial fluctuating value
" = purely time-dependent fluctuating value

Subscripts

R = relative to the rotor
n = component normal to the shock
r = radial component
r = rotor
red = reduced value
ref = reference value
rel = relative to the rotor (for a time averaged process)
s = stator
θ = azimuthal co-ordinate
τ = component tangent to the shock
1 = rotor inlet conditions

INTRODUCTION

A critical issue for the turbomachinery industry remains the time-averaged simulation of multi-stage turbomachinery. Classical 3D multi-blade row simulation methods consist in connecting results of stationary calculations applied to isolated adjacent blade rows, the information between the rows usually being exchanged through
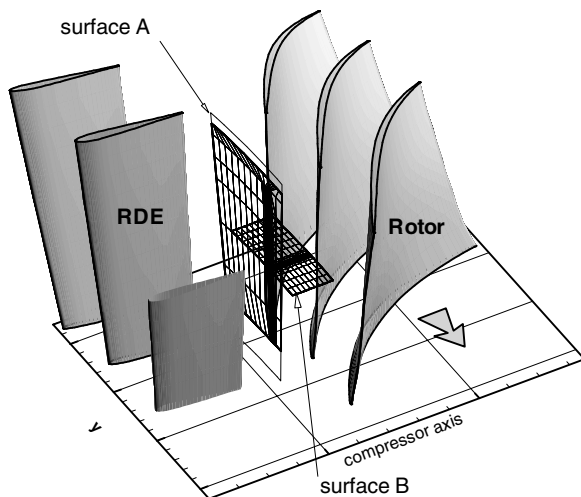
1

Fig. 1: data location

mixing planes. A circumferential averaging procedure yields time-averaged conditions along these inter-row planes. Nevertheless, unsteady blade-row interaction has repercussions on the time-averaged flow (Adamczyk et al., 1994, Hall, 1997, Rhie et al., 1995). Bardoux et al. (1998a) provide an interesting review of numerical results using mixing-plane methods and more complex approaches using deterministic correlation models. The authors highlight the shortcomings of such methods, which are mainly due to the fact that only spatial correlations are modeled. From time-dependent numerical results in a transonic turbine stage, they perform a direct computation of all the correlations in order to evaluate their influence on the time-averaged flow field. Regarding the experimental results available in the literature, few can be used to calculate these deterministic correlations. Thus, from the data bank obtained from the measurements performed in the inter-row region of a transonic compressor, our main subject of interest is the evaluation of the temporal correlations, which represent the unsteadiness of the flow. Without claiming to build any model for the computation of these correlations, we propose to give some clues to the orders of magnitude of the temporal correlations relative to the spatial correlations.

In the first part of this paper, the results of L2F measurements performed in the IGV-rotor inter-row region of a high-pressure ratio compressor were presented. They provide a detailed data bank for a comprehensive description of the inter-row flow field and for a validation of numerical simulations. It is pointed out that the flow field is dominated by the moving oblique shock emanating from the rotor blade leading edge and its interaction with the IGV wake.

In this second part of the paper, the experimental data in the compressor are further discussed, with special attention to the evolution of the IGV wakes, the shape and the location of the oblique shock wave emanating from the leading edge of the rotor blades and their interaction. If the twenty investigated azimuthal locations cover 110% of the IGV pitch and allow a good description of the IGV wakes in the absolute frame, they make up a field which is not wide enough to restore the whole flow field in the relative frame. Therefore, the spatial-temporal (chorochronic) periodicity (Erdos et al., 1977, Gerolymos and Chapin, 1991) is experimentally checked and applied to the data. Furthermore, the flow field is analyzed, in terms of temporal and spatial averaged values and fluctuating components,

using the decomposition developed by Adamczyk et al. (1986). The purely time-dependent velocity fluctuations especially are quantified.

IGV WAKE AND ROTOR OBLIQUE SHOCK

Measurements location

The data were collected in a section A normal to the free stream direction, and on a blade-to-blade surface B at 50% section height. At mid-span, section A is located at 31% of the IGV chord, downstream of the IGV trailing edge, and at 28% of the rotor chord, upstream of the rotor leading edge. The blade-to-blade surface B is described from section A up to the rotor leading edge region. The data location is given in Fig. 1.

Flow field decomposition

In addition to three-dimensional, turbulent and viscous effects, non-uniformities and unsteadiness due to the rotor-stator interaction introduce major complexity in the analysis of the flow field. This problem can be simplified by decomposing any flow variable $X(r,z,\theta,t)$ into averaged $\overline{X}$ and fluctuating X' components. Such decomposition can be applied either in the absolute frame or in the frame relative to the rotor. A first decomposition stage consists in writing:

$$X(r,z,\theta,t) = \overline{X}(r,z,\theta) + X'(r,z,\theta,t) \qquad (1)$$

$$\overline{X}(r,z,\theta) = \widetilde{X}(r,z) + \overline{X}^*(r,z,\theta) \qquad (2)$$

with

$X(r,z,\theta,t)$ the instantaneous value at any given location

$\widetilde{X}(r,z)$ the time and blade-to-blade averaged value (or axisymmetric value)

$\overline{X}^*(r,z,\theta)$ the blade-to-blade fluctuating component of the time-averaged value

$X'(r,z,\theta,t)$ the periodic temporal fluctuating component, clocked with the rotor frequency.

The fluctuating components are exclusively periodic because the L2F data acquired in each rotor blade channel are superimposed. Note that all the mean values are obtained with an arithmetic averaging process.

A further decomposition can be applied to this last term and will be expressed later.

The IGV wake

The measurements have been realized in the absolute frame and the investigated azimuthal locations, covering 110% of the IGV pitch, allow a good description of the IGV wakes. The measurements performed in section A lead to a description of the radial evolution of the stator wake. The feature of the wake is described by the blade-to-blade periodic fluctuating components of the time-averaged velocity in the absolute frame, $\overline{V}^*(r,z,\theta)$, and angle, $\overline{\alpha}^*(r,z,\theta)$. These components are shown in Fig. 2, versus the angular position normalized by the IGV pitch, for four immersion values. The wake width at 50% section height is about 10% of the stator blade pitch and,
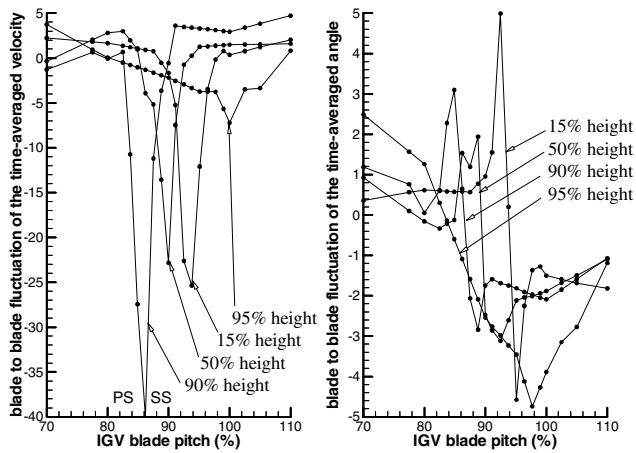
2   Copyright (C) 2000 by ASME

Fig. 2: blade-to-blade fluctuating components of the time-averaged velocity and angle, versus the angular position normalized by the IGV pitch, for four immersion values
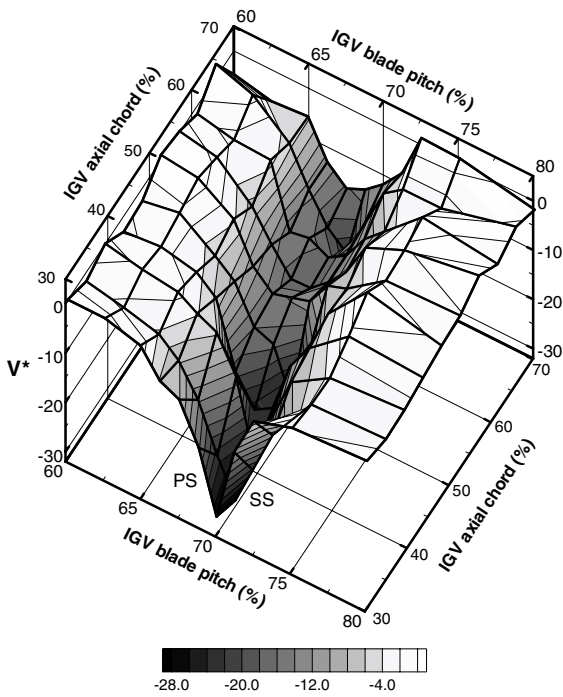

Fig. 3: streamwise evolution of the stator wake blade-to-blade fluctuating component of the time-averaged velocity at 50% of span

except at 95% of span, it remains more or less constant along the section. The maximum defect in velocity at 50% section height is 23m/s (i.e. 13% of the free-stream velocity), whereas it reaches 40m/s (i.e. 24% of the free-stream velocity) at 90%. From 15 to 90% of span, the angle evolutions indicate that the flow is over-turned (higher negative values) on the suction side and under-turned on the pressure side of the wake. This is consistent with the wake feature of an isolated
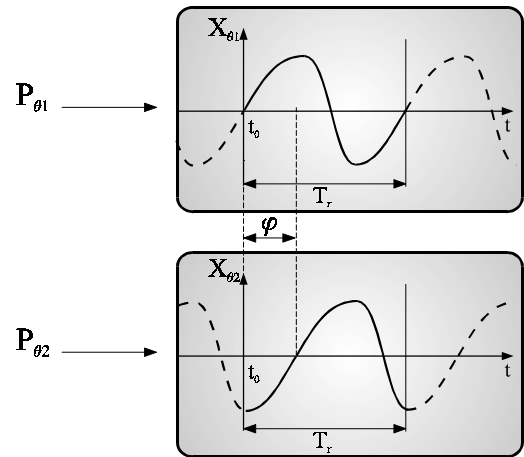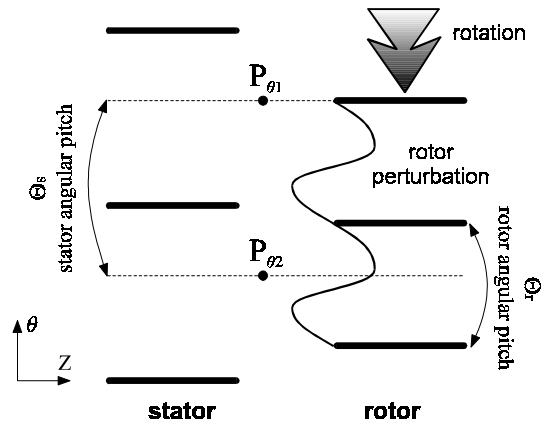

Fig. 4: illustration of the spatial-temporal periodicity

blade row. In the end-wall region (95% of span), the wake width is very large, which is probably partly due to the radial migration of low momentum stator blade boundary layer flow toward the shroud.

The streamwise evolution of the stator wake blade-to-blade fluctuating component of the time-averaged velocity, from section A up to the rotor leading edge, is drawn in Fig. 3, from the measurements performed at 50% of span (surface B). Along this distance (from 30% to 70% of the IGV axial chord, downstream of the trailing edge) the wake width slightly increases, whereas the maximum defect in velocity decreases down to half the value obtained in section A.

The rotor leading edge shock

In order to analyze the oblique shock wave emanating from the leading edge of the rotor blades, it is more suitable to make a transcription of the data obtained, in the frame relative to the rotating blade row. However, the field that has been investigated is not wide enough in the circumferential direction to restore the whole flow field in the relative frame, so hypothesis of spatial-temporal (chorochronic) periodicity is necessary. Such a procedure, which excludes distortions moving in the circumferential direction at a fraction of the rotor speed (rotating-stall for instance) and requires an axisymmetric upstream flow field, is usually applied in numerical simulations where the

3 Copyright (C) 2000 by ASME

calculations are performed in one channel only. It has been experimentally checked and applied to the obtained data.

Let us consider the IGV (stator) with N_s blades, and the rotor with N_r blades, of the investigated compressor. The time variations of any aerodynamic parameter $X_{\theta 1}(t)$ at a fixed point $P_{\theta 1}$ of the stator-rotor inter-row region are assumed to result from the perturbations arising from the rotor blades moving downstream (Fig. 4). Thus, the temporal period T_s of the measured signal X is connected to the spatial period of the rotor blade passage (blade pitch Θ_r), by its rotating speed ω ($\Theta_r = \omega \cdot T_s$). Let us now consider another point $P_{\theta 2}$ located at the azimuthal co-ordinate θ_2 such as $\theta_2 = \theta_1 - \Theta_s$ (where Θ_s is the stator angular pitch). Points $P_{\theta 1}$ and $P_{\theta 2}$ are defined as homologous. At $P_{\theta 2}$, signal $X_{\theta 2}(t)$ is under the same rotor perturbations, but phase-shifted:

$$X_{\theta_2}(t) = X_{\theta_1}(t - \varphi) \qquad (3)$$

So the hypothesis of the spatial-temporal periodicity consists in linearly linking the time and the circumferential distance. The phase shift φ is expressed by:

$$\varphi = \left(1 - \frac{N_r}{N_s}\right)\frac{\Theta_r}{\omega} \qquad (4)$$

The phase shift has been experimentally checked for two pairs of homologous points (located at 0% - 100% and 10% - 110% of the IGV pitch), and for each of the 10 axial locations investigated on surface B. That leads to an estimated mean value of φ (expressed as a percentage of the rotor temporal period T_r) of 17.5%. The theoretical value of φ, calculated with equation (4), is 19%. The small disparity observed between these two values can be attributed to the differences in shape of the signals resulting from the measurement uncertainties. We can therefore assume that the spatial-temporal periodicity is well verified.

Thus, by transcribing the L2F data in the relative frame, using this hypothesis of spatial-temporal periodicity, and by time-averaging the values in the relative frame, the mean inlet relative flow is restored. The contour map of the relative Mach number M_R at 50% of span (surface B) is presented in Fig. 5, where the abscissa is the axial distance expressed as a percentage of the rotor blade chord and the ordinate is the angular position normalized by the rotor pitch. The strong deceleration through the shock as well as the acceleration due to the expansion waves are clearly visible. The shock is nearly normal around the leading edge and turns oblique upstream.

An analysis of the shock pattern is proposed by means of the calculation of the "unique incidence condition", assuming a two-dimensional cascade flow with an axial subsonic velocity component. This calculation, which is valid for a started supersonic cascade with sharp blades, is extended to include the effects of detached shock waves in the case of a blunt leading edge (Lichtfuss and Starken, 1974). The total pressure losses, leading to a blockage factor, are obtained by integration along a pitch, assuming the shock wave degenerates to one Mach line upstream of the adjacent blade. The axial stream contraction is taken into account by means of an additional blockage factor, calculated from the geometric convergence of the channel. This procedure yields the inlet flow angle and the shape of the detached shock wave at a prescribed inlet flow Mach number. In the present case, the conditions upstream of the bow wave are not constant. The value of M_{R1} is therefore not known and is calculated by time averaging the Mach number at a point located in the wake-free
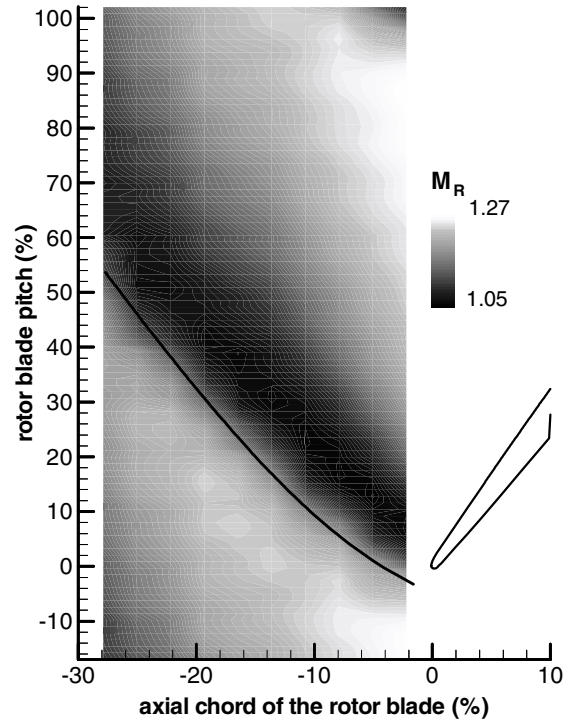

Fig. 5: contour map of the relative time-averaged Mach number at mid-span and analytical shock location
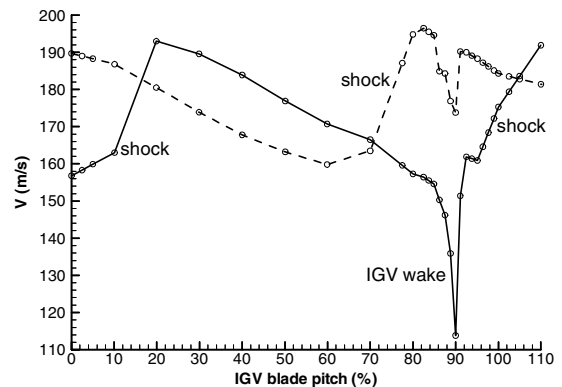

Fig. 6: two azimuthal evolutions of the absolute velocity at mid-span, for two different times

region of section A. This way of determining the relative inlet flow Mach number has been validated by Trébinjac and Claudin (1997). It leads in the present case to $M_{R1} = 1.14$. The calculation of the inlet flow angle leads then to $\beta_{cal} - \beta_{mes} = 0.3°$. The agreement is all the better as the difference value is within the measurement errors. The predicted shape of the shock wave is superimposed onto the experimental results in Fig. 5. The calculated detachment distance is 0.8 mm whereas it is experimentally estimated to be 0.7 mm. All these analytical results are very satisfactory in spite of the simplifying assumptions. Moreover, such a simple integral method is a useful tool for predicting the flow zones which require an over-refinement of the mesh, experimentally and numerically speaking.
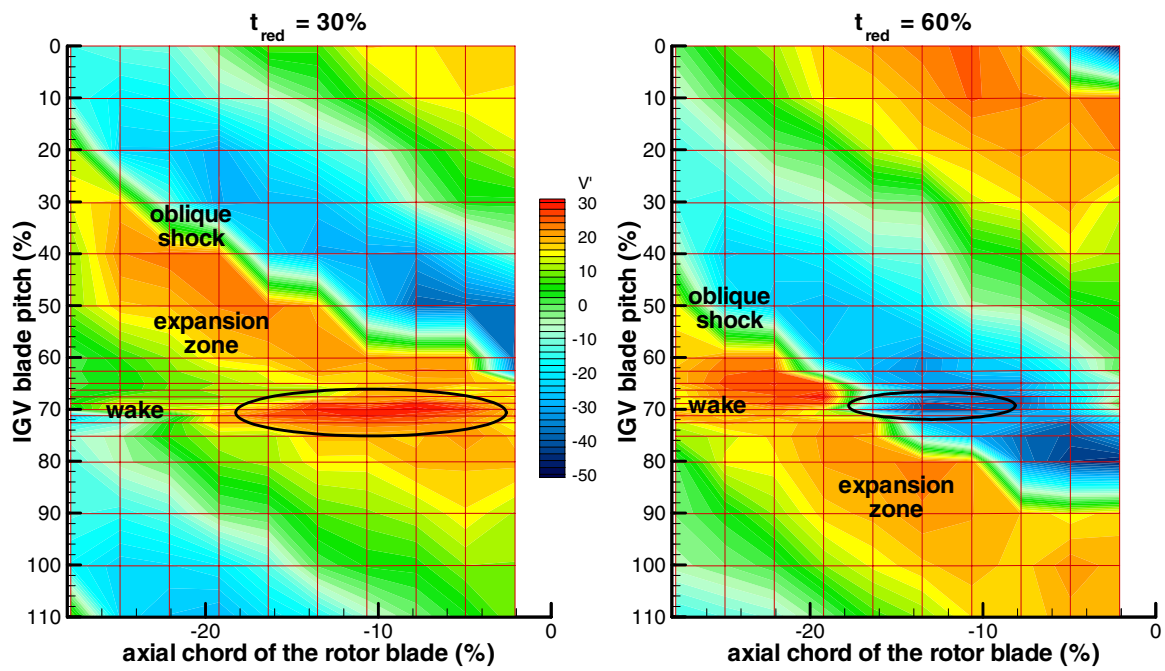
4

Fig. 7: contour map on surface B of the temporal fluctuating component of the velocity for two different times
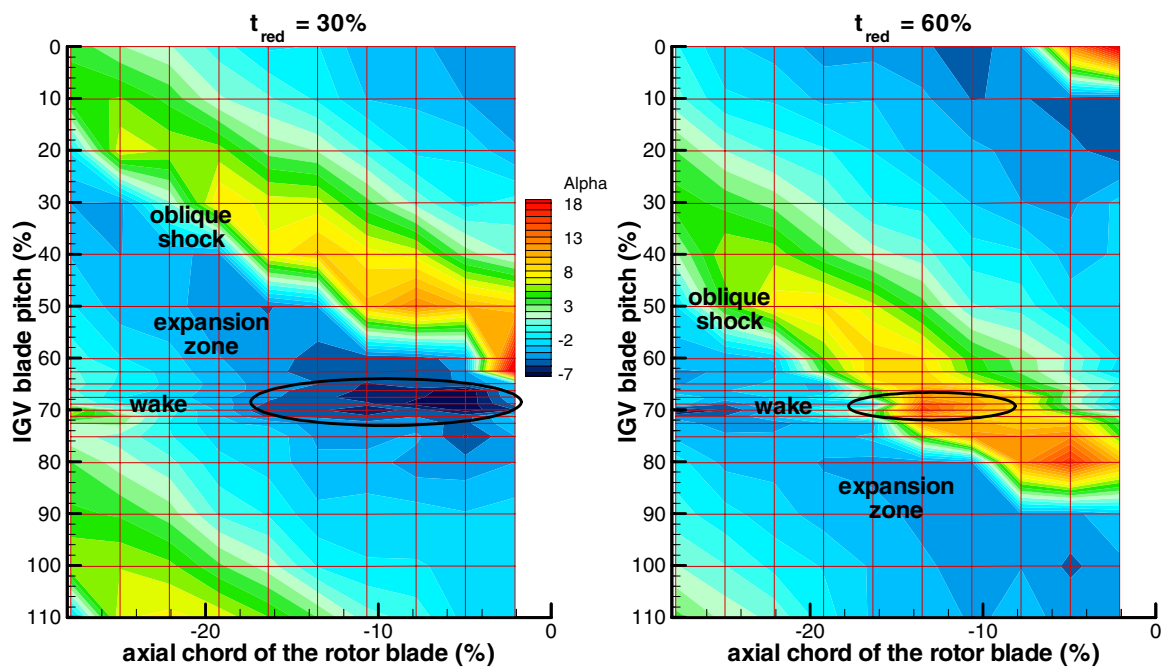

Fig. 8: contour map on surface B of the temporal fluctuating component of the angle for two different times

5

IGV wake and oblique shock interaction

The time-dependent behavior of the IGV wake, interacting with the shock, is presented in part 1 of the paper and is briefly illustrated in Fig. 6, by comparing the azimuthal evolutions of the instantaneous velocity for two times (i.e. positions of the rotor row relative to the IGV). In this example, the axial location of the data is very close to section A.

The time-averaging process used above isolates the wake (by averaging in the absolute frame of reference) or the shock (by averaging in the relative frame). The effects of the shock/wake interaction are now evaluated by quantifying the temporal fluctuating components of the velocity and the angle. If the temporal fluctuations are calculated in the absolute frame, the effect of the moving shock on the wake feature can be quantified. Amongst all the results obtained on surface B for ten positions of the rotor blade row, two contour maps of the temporal fluctuating components of the velocity, $V'(r,z,\theta,t)$, and angle, $\alpha'(r,z,\theta,t)$, are extracted for two times (i.e. two positions of the row) highlighting the shock/wake interaction. These maps are presented in Fig. 7 and 8 where the abscissa is the axial distance expressed as a percentage of the rotor blade chord and the ordinate is the angular position normalized by the IGV pitch. In both figures, regarding the encircled zone, case (a) corresponds to a time before the shock has crossed the wake ($t_{red}=(t-t_{ref})/T_r=30\%$) whereas case (b) corresponds to a time just after the passage of the shock ($t_{red}=60\%$). In case (a), the wake is mainly in the expansion region and fluctuations V' reach high positive values. This means that the wake is accelerated more by the expansion waves than is the wake-free flow, and the magnitude of the wake will decrease before passing through the shock. In case (b), fluctuations V' in the wake reach high negative values after passing through the shock, so the wake deepens below the shock. Regarding fluctuations α' (Fig. 8), the flow within the wake comes under higher deviations than the free-wake flow (higher negative values of α' before the shock and greater positive values after the shock).

Moving downstream, the level of the fluctuations, averaged in the wake, globally increases by 50%. But that does not mean the interaction is stronger because a great part of the fluctuations arises from the increasing strength of the shock when approaching the leading edge of the rotor blades. By decomposing these fluctuations, as proposed below, the part due to the shock can be separated from the part due to the interaction proper.

Thus, the shock wave modifies the wake, which is a low momentum fluid zone, much more than the wake-free flow. Such behavior is corroborated by analyzing the evolution of the stationary wake vorticity through the moving oblique shock. The vorticity transport equation, for compressible viscous flow, derives from the application of the rotational operator on the momentum equation. In the absolute frame, it is written as follows:

$$\frac{\partial \vec{\Omega}}{\partial t} + \left(\vec{V}\cdot\overrightarrow{\text{grad}}\right)\vec{\Omega} - \left(\vec{\Omega}\cdot\overrightarrow{\text{grad}}\right)\vec{V} = \frac{\vec{\Omega}}{\rho}\cdot\frac{d\rho}{dt} - \overrightarrow{\text{grad}}\frac{1}{\rho}\wedge\overrightarrow{\text{grad}}\,p$$
$$+ \overrightarrow{\text{rot}}\left(\frac{1}{\rho}\cdot\text{div}\left(\bar{\bar{\tau}}\right)\right) + \overrightarrow{\text{rot}}\,\vec{f} \quad (5)$$

where:

$$\frac{d\rho}{dt} = \frac{\partial\rho}{\partial t} + \vec{V}\cdot\overrightarrow{\text{grad}}\,\rho \quad (6)$$
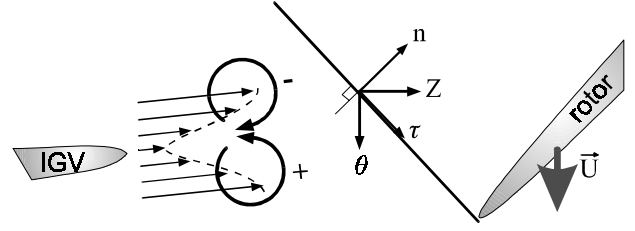

Fig. 9: schematic description of a moving shock wave interacting with the vorticity linked with a wake

In order to quantify the effect of the oblique shock on the vorticity of the wake, the most convenient co-ordinate system is co-ordinate system $(\vec{n},\vec{r},\vec{\tau})$ where $\bar{n}$ and $\vec{\tau}$ are respectively the unit direction vectors normal and tangent to the shock (Fig. 9). The pattern of the oblique shock, emanating from the rotor blade leading edge and extending upstream of it, is assumed to be imposed by the wake-free incoming supersonic flow. Its moving in the circumferential direction is taken into account by the time derivative of the fluid density in the absolute frame. This time fluctuation is clocked with the rotor blade-passing frequency and can thus be written as:

$$\frac{\partial\rho}{\partial t} = \frac{\delta\rho}{\delta t} - \vec{U}\cdot\overrightarrow{\text{grad}}\,\rho \quad (7)$$

with $\dfrac{\delta\rho}{\delta t}$ the time derivative of the density in the relative frame.

If the wake is assumed to be two-dimensional, its velocity field is described in the $(\vec{n},\vec{r},\vec{\tau})$ co-ordinate system by two components, $V_n(n,\tau)$ and $V_\tau(n,\tau)$. The associated component of the vorticity is:

$$\Omega_r = -\frac{\partial V_\tau}{\partial n} + \frac{\partial V_n}{\partial \tau} \quad (8)$$

Using this modelisation and neglecting the terms representative of the non-stationarity of the density field in the relative frame, the external forces and the turbulent and viscous stress tensor in the basic equation, the change in Ω_r can be written as:

$$\frac{d\Omega_r}{dt} = -\frac{1}{\rho}\cdot\frac{\partial V_n}{\partial\tau}\cdot\frac{\partial V_n}{\partial n}\left(U_n + V_n\right) \quad (9)$$

It is clear from this equation that the change in Ω_r is brought by a stationary term and a non-stationary term by the normal component of rotor speed U_n. These two effects are cumulative and lead to an increase in the magnitude of vorticity Ω_r, whatever its sign.

Figure 10 shows the contour map of the radial component Ω_r of the vorticity, calculated from the experimental data. The ordinate is the angular position normalized by the IGV pitch and the abscissa is the time expressed as a percentage of the rotor pitch time, but two periods are placed side by side to make it clearer. The shock region is marked off by low positive values of the magnitude of Ω_r, whereas the wake boundaries are characterized by high values. The increase in magnitude of Ω_r in the interaction zone of the wake with the moving oblique shock, is clearly visible. This corroborates, as mentioned above, that the wake deepens below the shock.
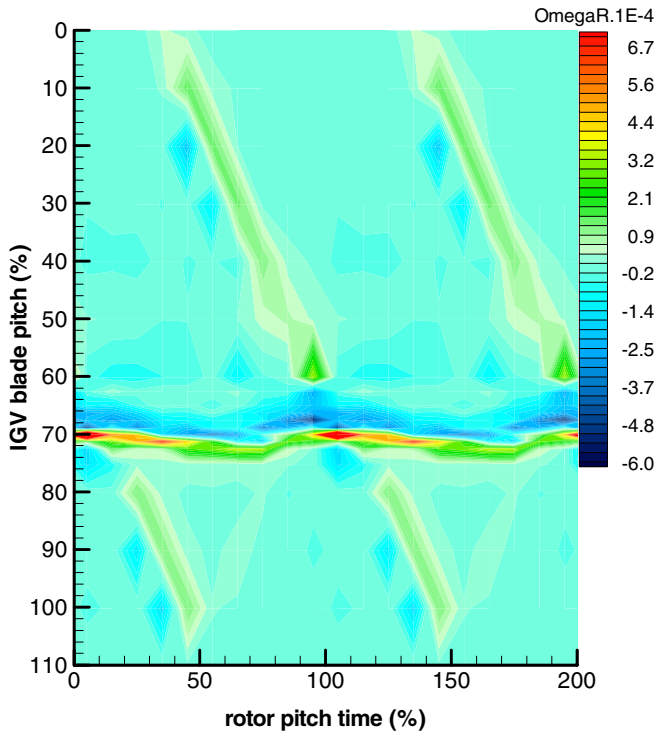
6

Copyright (C) 2000 by ASME

Fig. 10: contour map of the radial component Ω_r of the of the vorticity calculated from the experimental data

PURELY TIME-DEPENDENT VELOCITY FLUCTUATIONS

Adamczyk decomposition

As mentioned above, a discriminating decomposition of the periodic temporal fluctuating component in the absolute frame, $X'(r,z,\theta,t)$, is achieved in order to extract the effect of the shock/wake interaction proper. This decomposition was proposed by Adamczyk (1986):

$$X'(r,z,\theta,t) = \overline{X}^*_{rel}(r,z,\theta) + X''(r,z,\theta,t) \qquad (10)$$

Then:

$$X(r,z,\theta,t) = \widetilde{\overline{X}}(r,z) + \overline{X}^*(r,z,\theta) + \overline{X}^*_{rel}(r,z,\theta) + X''(r,z,\theta,t) \qquad (11)$$

The first two terms are those resulting from the previous stage of the decomposition (2), in the absolute frame. $\overline{X}^*_{rel}(r,z,\theta)$ is the spatial fluctuation of the time-averaged flow in the frame relative to the rotor. $X''(r,z,\theta,t)$ is a purely time-dependent fluctuation which arises from the interaction of phenomena occurring in different frames. This term is also called "deterministic fluctuation", as opposed to the random (or non-deterministic) fluctuation which arises from the turbulence and other phenomena not clocked with the rotor frequency. In the present decomposition applied to the experimental values, the random part is excluded because it is already averaged by the acquisition and reduction procedures that lead to the mean values of the modulus and angle of the velocity vector. Nevertheless, it is taken into account in the values of the standard deviation. Regarding

$$V(r,z,\theta,t) = \widetilde{\overline{V}}(r,z) + \overline{V}^*(r,z,\theta) + \overline{V}^*_{rel}(r,z,\theta) + V''(r,z,\theta,t)$$
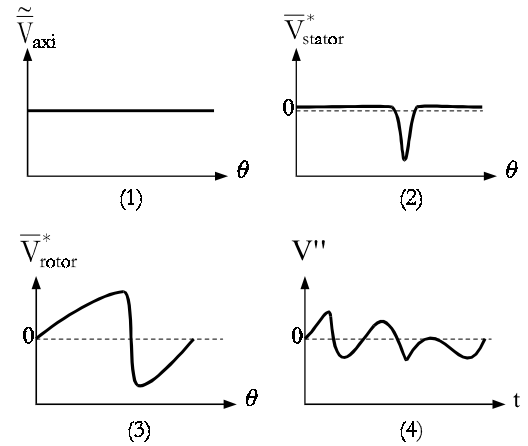$$\qquad (1) \qquad\qquad (2) \qquad\qquad (3) \qquad\qquad (4)$$

Fig. 11: comprehensive sketch of the Adamczyck decomposition of the velocity
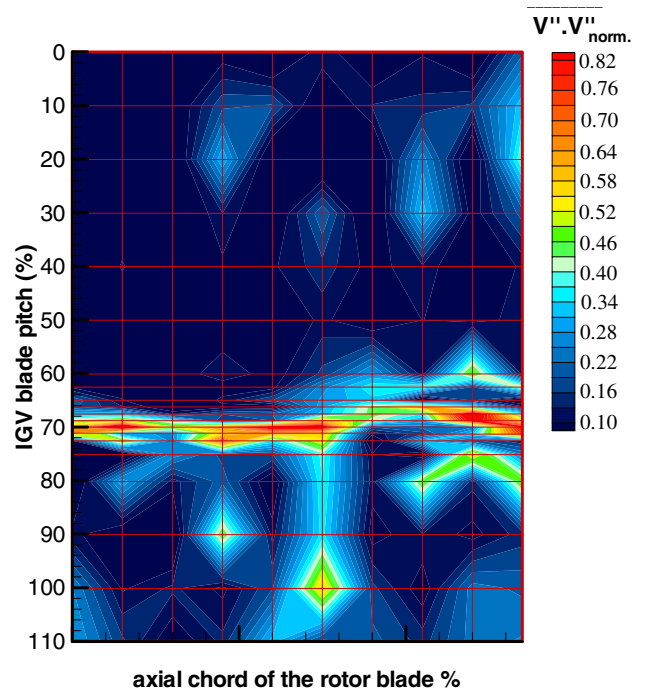

Fig. 12: contour map of the normalized unsteady correlations

the numerical approaches using such a decomposition, this random part is also excluded because it is assumed to be modeled by a turbulence model. A comprehensive sketch of the decomposition of the instantaneous velocity modulus is proposed in Fig. 11, in order to illustrate the different physical meanings of each term.

The time-dependent L2F data enable the calculation of each of the four terms of the decomposition of the modulus and angle of the velocity vector. From the periodic temporal fluctuating component of

7   Copyright (C) 2000 by ASME

the velocity in the absolute frame, $V'(r,z,\theta,t)$, the stator deterministic correlation, which represents the averaged consequence of unsteady phenomena, can be calculated. This correlation can be decomposed into a purely spatial part, two spatial-temporal parts and a purely unsteady part:

$$\overline{V'(r,z,\theta,t) \cdot V'(r,z,\theta,t)} = \overline{\overline{V}_{rel}^*(r,z,\theta) \cdot \overline{V}_{rel}^*(r,z,\theta)} \\ + \overline{\overline{V}_{rel}^*(r,z,\theta) \cdot V''(r,z,\theta,t)} \\ + \overline{V''(r,z,\theta,t) \cdot \overline{V}_{rel}^*(r,z,\theta)} \\ + \overline{V''(r,z,\theta,t) \cdot V''(r,z,\theta,t)} \quad (12)$$

Let us mention that, in the various models that handle the interaction between blade rows, all the correlations, except the purely spatial one, are usually neglected.

Results

The purely time-dependent correlation $\overline{V''(r,z,\theta,t) \cdot V''(r,z,\theta,t)}$ has been calculated from the L2F results on surface B. The values obtained are normalized by the spatial correlation $\overline{\overline{V}_{rel}^*(r,z,\theta) \cdot \overline{V}_{rel}^*(r,z,\theta)}$ induced by the shock wave in section A, which is about 122 m^2/s^2. The contour map of the normalized unsteady correlation is shown in Fig. 12, where the abscissa is the axial distance expressed as a percentage of the rotor blade chord and the ordinate is the angular position normalized by the IGV pitch. As expected, the high levels are located within the wake, where the unsteady correlation reaches 80% of the maximum spatial correlation. It remains more or less constant from section A up to the leading edge of the rotor blades. That means the increase in the temporal fluctuations $V'(r,z,\theta,t)$ mentioned above, when moving downstream, is mainly due to the increase of the spatial velocity fluctuation of the rotor time-averaged flow ($\overline{V}_{rel}^*(r,z,\theta)$), which is only due to the increase of the strength of the shock when approaching the leading edge of the rotor blades, and not of the interaction proper (i.e. the unsteady fluctuations).

These results show that the purely unsteady part of the deterministic correlations is of the same order of magnitude as the spatial part. But the relative strengths of the various parts of the deterministic correlations have been quantified only in the inlet rotor flow field. In this region, the sources of unsteadiness are certainly of less importance than within the rotor blade row (unsteadiness due to the normal passage shock, the blade boundary layers, the secondary flows and all the interactions). Then, the temporal correlations may be assumed to increase still further within the rotor, and should not be neglected in the 3D rotor time-averaged simulations.

A numerical study of the time-averaged flow in a transonic single-stage turbine, realized by Bardoux et al. (1998b), led to similar conclusions. The authors demonstrate that the temporal correlations are of a greater order of magnitude than the spatial correlations inside the rotor. These temporal correlations illustrate the oscillation of the rotor passage vortices and the chopping of the stator wakes.

To return to the present investigation in the compressor, future work should include measurements within the rotor and the analysis of a three-dimensional unsteady simulation, thus confirming the significant role of temporal correlations compared to spatial correlations.

CONCLUSION

By analyzing the time-dependent L2F results obtained in the inter-row flow field of a transonic compressor stage, the effects of the rotor leading edge shock wave/IGV wake interaction can be evaluated. This analysis is performed by implementing tools usually used in numerical works, to reduce the experimental data.

A comprehensive description of both the IGV wake and the shock emanating from the leading edge of the rotor is made. The experimental shock pattern is compared with the shock pattern deduced by an integral method. The very good agreement means the analytical calculation can be considered as an easy and quick tool for giving information, useful for the initialization of numerical simulations.

The effect of the shock/wake interaction proper is quantified by calculating the purely time-dependent correlation occurring in the Adamczyk decomposition. This temporal correlation proves to be of the same order of magnitude as the spatial correlation. That tends to prove that temporal correlations should be considered in the 3D rotor time-averaged simulations, so as they will probably increase inside the rotor.

REFERENCES

Adamczyk, J.J., Mulac, R.A., Celestina, M.L., 1986, "A Model for Closing the Inviscid Form of the Average-Passage Equation System", *ASME Paper* 86-GT-227.

Adamczyck, J.J., Celestina, M.L., Chen, J.P., 1994, "Wake Induced Unsteady Flows: Their Impact on Rotor Performance and Wake Rectification", *ASME Paper* 94-GT-219.

Bardoux, F., Dano, C., Leboeuf, F., and Toussaint, C., 1998a, "Characterization of Deterministic Stresses for a Turbine Stage – Part 1: Steady Flow Analysis", *ASME Paper* 99-GT-100, pp 1-9.

Bardoux, F., Dano, C., Leboeuf, F., and Toussaint, C., 1998b, "Characterization of Deterministic Stresses for a Turbine Stage – Part 2: Unsteady Flow Analysis", *ASME Paper* 99-GT-101, pp 1-8.

Erdos, J.I., Alzner, E., and McNally, W., 1977, "Numerical Solution of Periodic Transonic Flow through a Fan Stage", *AIAA Journal*, 15, pp. 1559-1568.

Gerolymos, G.A., Chapin, V., 1991, "Generalized Expression of Chorochronic Periodicity in Turbomachinery Blade Row Interaction", *La Recherche Aerospatiale*, 5.

Hall, E.J., 1997, "Aerodynamic Modeling of Multistage Compressor Flow Fields. Part II: Modeling Deterministic Correlations", *ASME Paper* 97-GT-345.

Lichtfuss, H.J., and Starken, H., 1974, "Supersonic Cascade Flow", *Progress in Aerospace Sciences*, vol.15, edited by D.Küchemann, Pergamon Press.

Rhie, C.M., Gleixner, A.J., Spear, D.A., Fischberg, C.J., Zacharias, R.M., 1995, "Development and Application of a Multistage Navier-Stokes Solver. Part I: Multistage Modeling using Bodyforces and Deterministic Stresses", *ASME Paper* 95-GT-342.

Trébinjac, I., and Claudin, I., 1997, "Results and Analysis of a L2F Flow Field Investigation within a High-Speed High-Pressure Centrifugal Compressor", *International Journal of Thermal and Fluid Sciences*, vol.6, nb 3, pp 155-163.